scientific reports

Check for updates

OPEN

Investigating the kinetics of single-chain expansion upon release in theta conditions

Pai-Yi Hsiao[1,2]✉

The free expansion of a confined chain in theta solvents following a sudden removal of the confining constraint is investigated using Langevin dynamics simulations in both two- and three-dimensional spaces. The average evolution of the chain size exhibits a sigmoidal transition between the confined and the free states on a logarithmic timescale, indicating a two-stage expansion, each characterized by its own timescale. A kinetic theory is developed by applying Onsager's variational principle, which balances the change in free energy with energy dissipation. Through scaling analysis, the characteristic time τ_1 for the first expansion stage is shown to scale as the cube of the initial chain size, while the chain size increases according to a power law with an exponent $\alpha_1 = 1/3$, independent of the spatial dimension. In the second stage, the timescale τ_2 is found to be proportional to the square of the chain length, and the evolution of the chain size follows an exponential recovery function powered by an exponent $\alpha_2 = 1/4$. These results are further validated by a direct analysis of the kinetic equations via simulations. Moreover, the general forms of the free energy for the two expansion stages are established through the integration of the kinetic equations. Finally, physical interpretations are proposed, employing a radial expansion model and a diffusive mechanism to explain the observed scaling behaviors. This work explores a model system under the specific solvent condition, providing foundational theory and enhancing our understanding of the expansion-upon-release phenomenon.

In nature, genetic materials are often packaged into small volumes or particles, such as chromatin condensed within a nucleus and DNA or RNA chains confined in viral capsids[1–3]. Understanding the mechanisms of unpacking or unconfining these materials is essential for comprehending the functions and replication processes in cells and in microbiology. A similar approach is utilized in nanotechnology where DNA chains or drugs can be encapsulated into nanoparticles or confined within specific regions, enabling targeted delivery for therapeutic applications[4–9]. In this study, we address the problem by examining a fundamental process, the free expansion of a single chain abruptly released from a confining state under a specific solvent condition.

A closely related area of research is known as the globule-to-coil transition, which involves the transformation of a chain from a globule state in a poor solvent to a coil state by enhancing the solvent quality. While significant efforts have been dedicated to understanding the opposite process, namely the "coil-to-globule" transition, since the 1960s[10–23], there has been comparatively less focus on the globule-to-coil transition[24–29]. The first observation of the globule-to-coil transition of single chains was made by Wu and co-workers[30,31]. They discovered that the transition is irreversible and exhibits hysteresis in the evolution of chain size due to the cyclic decrease and increase of temperature. Pitard and Orland[32] theoretically investigated the swelling dynamics of a polymer quenched from a theta solvent to a good solvent. The chain size was predicted to evolve as $R^2(t) \simeq R^2(0)\left(1+\left(\frac{t}{\tau_c}\right)^{3/4}\right)$ with the characteristic time $\tau_c \sim N^{4/3}$ at the beginning, and then transition to an exponential recovery as $R(t) \sim N^{3/5}\left(1-\exp\left(-\frac{t}{\tau_1}\right)\right)$ with $\tau_1 \sim N^{11/5}$ subsequently. Lee et al.[33,34] discussed the effects of hydration and chain self-entanglement. They predicted a power-law scaling of $R(t) \sim t^{1/5}$ and $t^{2/5}$ for chain swelling from a fresh-wet and a fresh-dry globule, respectively. If the globule is wet and entangled, the chain first evolves rapidly to reach an arrested state with a time scale of about $t_a \sim N^{2/3}$, and then disentangles and swells to attain its final size with a dominant duration of time estimated to be $t_d \sim N^2$. If the entangled globule is dry, reptation becomes the key dynamic process for disentangling the chain and the swelling time should be roughly N^3. Sakaue and Yoshinaga[35] assumed a balance of the rate of the free energy change with the energy

[1]Department of Engineering and System Science, National Tsing Hua University, Hsinchu, Taiwan, R.O.C.. [2]Institute of Nuclear Engineering and Science, National Tsing Hua University, Hsinchu, Taiwan, R.O.C.. ✉email: pyhsiao@ess.nthu.edu.tw; pyhsiao@mx.nthu.edu.tw

dissipation during the expansion and solved the kinetic equation. The evolution of chain size was predicted: $R(t) \simeq R_0 \left(1 + \frac{t}{\tau_{\rm ini}}\right)^{\alpha}$, where $\alpha = \frac{3\nu-1}{9\nu}$ with $\nu = \frac{3}{5}$ being the Flory exponent, and $\tau_{\rm ini} \simeq \tau_0 \left(\frac{R_0}{aN^{1/3}}\right)^{1/\alpha}$. Experiments[36,37] have observed that the expansion size in a globule-to-coil transition can be approximately described by $R^2(t) = R_{\rm eq}^2 - (R_{\rm eq}^2 - R_0^2)\exp\left(-\left(\frac{t}{\tau}\right)^{\beta}\right)$ with R_0 and $R_{\rm eq}$ being the initial and final chain sizes and β a fitting parameter.

There are, however, subtle differences between the phenomena of the globule-to-coil transition and the expansion of a confined chain upon release. In the former case, the transition is triggered by a reduction in the internal interactions between chain segments due to improvement in solvent quality. In contrast, the latter involves a thermodynamic process in which a chain returns to a free state in a solution after the removal of external forces or constraints. Since the internal interactions are not altered, the segment distribution and topological structure of a confined chain can differ remarkably from those in the former case, resulting in different types of expansion dynamics. Recently, we investigated the kinetics of the expansion-upon-release process in a good solvent in both three-dimensional (3D) and two-dimensional (2D) spaces[38,39]. By equating the free energy change with the energy dissipation, we developed a two-stage theory to explain the phenomenon. In the first stage, the chain undergoes explosive expansion while maintaining a spherical shape. The evolution of size, $R(t) = R_0 \left(1 + \frac{t}{\tau_1}\right)^{\alpha_1}$, was predicted, with the exponent $\alpha_1 = \frac{d\nu_b - 1}{2(d\nu_b - 1) + d}$ and the characteristic time $\tau_1 \sim N^{\frac{2}{d}+\chi_1}\phi_0^{-\frac{1}{d\alpha_1}}$, where d is the spatial dimension, and ν_b and ϕ_0 are the Flory exponent and volume fraction of the chain in the initial confinement, respectively. In the second stage of expansion, the chain adopts a coil conformation, and the evolution becomes $R(t) = R_{\rm eq}\left(1 - \exp\left(-\frac{t}{\tau_2}\right)\right)^{\alpha_2}$ with $\alpha_2 = \frac{1}{d+2}$ and $\tau_2 \sim N^{2+\chi_2}$. Here, the exponents χ_1 and χ_2 are related to the effective friction coefficient associated with the expansion speed in the two stages. The results have been confirmed through extensive computer simulations. Notably, universal kinetics of expansion were discovered by using suitable time and length scales in each stage[39]. The expulsion of a DNA chain from an icosahedral virus has been investigated by other groups using molecular dynamics simulations[40–42]. The authors revealed that the viral capsid opens with a large hole, facilitating the rapid release of the genome within microseconds. Our simulations demonstrated a similar timescale required for a free expansion process[38].

In a theta solvent, the excluded volume effect in polymers is canceled out by the interactions with the solvent. As a result, measured characteristics of the polymer chains become independent of the solvent. Physicists have developed various models, including freely-jointed chains, freely-rotating chains, worm-like chains, Gaussian chains, and others, to understand the properties of ideal chains under theta conditions[43]. This condition serves as an important framework for testing theoretical models and refining our understanding of polymer physics. For example, the average size of an ideal chain is known to scale as $\ell N^{1/2}$, corresponding to the mean displacement in an N-step random walk[44]. The quadratic entropic term used in the general free energy of a single chain arises from the Gaussian probability distribution of the size of an ideal chain[24,43]. The stretching behavior of a DNA chain can be approximated by the Marko–Siggia formula derived from the worm-like chain model[45]. Theta conditions also enhance our understanding of the diverse transport properties of polymer solutions[44,46]. Ideal chain statistics have been applied to explain the behavior of polymers in dense states or melts, to develop blob theories at different length scales, and to study the dynamics of entangled polymers[24,43]. These facts underscore the crucial role of ideal chains in modeling and analyzing a variety of polymer systems.

So far, studies related to the recovery kinetics of a confined chain upon release in theta conditions have been scarce, and a compelling theory to explain this phenomenon is still lacking. In this work, we investigate the model system using a freely-jointed chain, where a chain confined in a cavity is suddenly released to return to its natural state in a theta solution. A key question to be addressed is whether the two-stage theory previously developed for chain expansion in good solvents can be extended to the scenario in theta solvents. What are the scaling properties of the theta expansion, including any existing characteristic times and exponents? Comparing the results in theta solvents with those in good solvents allows us to gain insight into the effects of excluded volume on the expansion process. The structure of the paper is organized as follows: In section "Theory", we develop a general theory for the theta expansion of a confined chain using Onsager's variational principle. We then examine the predictions by performing Langevin dynamics simulations in both 3D and 2D settings, described in section "Model and setup". The topics studied include the evolution of chain size (section "Evolution of chain size"), the variation in chain shape (section "Variation of chain shape"), the scaling analysis of the evolution curves (section "Time scaling of $\tilde{R}_1$ and $\tilde{R}_2$"), the characteristic times and exponents (section "Characteristic times τ_1 and τ_2 and exponents α_1 and α_2"), the expansion speed (section "Expansion speed"), and the verification of the kinetic equations (section "Kinetic equations"). Since the free energy can be obtained by integrating energy dissipation, our simulations allow for a direct examination of the free energy formulation used in the theory for the two expansion stages (section "Scaling form of free energy"). Finally, the conclusions and discussions are provided in section "Conclusions and discussions".

Theory

We study the expansion kinetic of an ideal chain released from a confining cavity in d-dimensional space. The cavity is a sphere if $d = 3$, while it is a disk if $d = 2$. The process is started by suddenly removing the confining constraint. We assume that the system is subject to Langevin dynamics. The problem can be studied by using Onsager's variational principle[47,48] by minimizing the functional $\mathcal{R}[\dot{R}] = \frac{1}{2}\eta_{\rm eff}\dot{R}^2 + \frac{{\rm d}F}{{\rm d}R}\dot{R}$, called

the Rayleighian, with respect to $\dot{R}$, the time derivative of the chain size R, where η_{eff} is the effective friction coefficient associated to $\dot{R}$, and F is the free energy of the system. The kinetic equation is thus obtained

$$\frac{\mathrm{d}R}{\mathrm{d}t} = -\frac{1}{\eta_{\text{eff}}}\frac{\mathrm{d}F}{\mathrm{d}R}, \tag{1}$$

which can also be derived from a balance of energy between the rate of change of free energy and the rate of energy dissipation, given by $\frac{\mathrm{d}F}{\mathrm{d}t} = -\eta_{\text{eff}}\left(\frac{\mathrm{d}R}{\mathrm{d}t}\right)^2$.

At the beginning of the process, the compressed chain undergoes a fast expansion by maintaining the chain conformation as a spherical globule . We call it "globule expansion". The free energy of the system is estimated to be $F \sim k_{\mathrm{B}}T\left(\ell N^{\nu}/R\right)^{1/\nu}$ where N is the number of segments on the chain and ℓ is the segment length. It is computed by counting the number N/g of the blobs formed in the globule of size R, each of which comprises g segments determined by the scaling relation $R \sim \ell g^{\nu}$ and possesses an energy of about $k_{\mathrm{B}}T$. We remark that the blobs are overlapped in the globule under the ideal-chain condition (Note: In polymer physics, a chain is conceptually divided into a series of small sections referred to as blobs. The statistical properties of the chain segments within a blob are unaffected by external constraints and exhibit scaling behavior described by $\xi \sim lg^{\nu}$, where ξ represents the blob size, g is the number of segments in a blob, and ν is the Flory exponent corresponding to the solvent conditions. Using the blob concept, we estimate the free energy F of a globular chain as $F \sim k_BT(N/g)$, where N/g counts the number of blobs and a blob has a free energy of about $k_{\mathrm{B}}T$ due to thermal interactions in the solvent environment. In a good solvent, the blobs are distinct because of the excluded volume interactions. Consequently, the number N/g can be approximated by $(R/\xi)^d$, where R is the globule size. From this approximation, we can derive the free energy as $F \sim k_BT\left(\frac{lN^{\nu}}{R}\right)^{d/(d\nu-1)}$. In the theta solvent considered here, where the ideal-chain condition permits blob overlap, the blob size ξ can become as large as the globule size R. Therefore, we have $F \sim k_BT\left(\frac{lN^{\nu}}{R}\right)^{1/\nu}$.). The kinetic equation Eq. (1) can be solved and the solution is

$$R(t) \simeq R_0\left(1 + \frac{t}{\tau_1}\right)^{\alpha_1} \tag{2}$$

where R_0 is the initial chain size, τ_1 is the the characteristic time, and α_1 is the power-law exponent. Under the assumption of Rouse dynamics $\eta_{\text{eff}} = \eta_0 N$, we have $\alpha_1 = 1/(2+\nu^{-1})$ and $\tau_1 \sim \frac{\eta_0\ell^2}{k_{\mathrm{B}}T}\left(\frac{R_0}{\ell}\right)^{1/\alpha_1}$. It predicts $\alpha_1 = 1/4$ and the scaling $\tau_1 \sim R_0^4$ by using $\nu = 1/2$. However, η_{eff} is an effective friction coefficient associated to the the state speed $\dot{R}$ in the kinetic equation. It can take a more complicated form with an additional dependence on the state variable R. A conjecture of $\eta_{\text{eff}} \sim \eta_0 N\left(\frac{R}{\ell}\right)^{y_1}$ will yield $\alpha_1 = 1/(2+\nu^{-1}+y_1)$ and deviate the scaling for τ_1 from the basic R_0^4-dependence to the $R_0^{4+y_1}$-dependence.

In the next stage, the chain gradually changes its conformation to adopt a coil shape and continues to expand toward its natural size in the bulk solution. This process is referred to as "coil expansion". The free energy of the chain in the coil state should not take the conventional form of Flory free energy, given by $F \sim k_{\mathrm{B}}T\left[\frac{R^2}{N\ell^2} + \frac{v_{\text{ex}}N^2}{R^d}\right]$, because the excluded volume v_{ex} is zero under theta conditions. A possible replacement for the free energy is $F \sim k_{\mathrm{B}}T\left[-\ln R + \frac{R^2}{N\ell^2}\right]$. This expression is derived from the Gaussian chain model, where $P(R) = \mathcal{A}_d \times \left(\frac{2\pi N\ell^2}{d}\right)^{-d/2}\exp\left(-\frac{dR^2}{2N\ell^2}\right)$ represents the probability distribution for having a chain size of R. Here $\mathcal{A}_d$ is the surface area of a sphere with radius R, equal to $4\pi R^2$ for $d = 3$ and $2\pi R$ for $d = 2$. Plugging the free energy into Eq. (1), we have the kinetic equation $\frac{\mathrm{d}R}{\mathrm{d}t} + \frac{k_{\mathrm{B}}T}{\eta_{\text{eff}}N\ell^2}R \sim \frac{k_{\mathrm{B}}T}{\eta_{\text{eff}}}R^{-1}$. The solution is

$$R(t) \simeq R_f\left(1 - C\exp\left(-\frac{t}{\tau_2}\right)\right)^{\alpha_2} \tag{3}$$

with $R_f \sim \ell N^{1/2}$, $\alpha_2 = \frac{1}{2}$, and $\tau_2 \sim \frac{\eta_{\text{eff}}N\ell^2}{k_{\mathrm{B}}T}$. The parameter C can be set to 1 because for a chain released from a highly compressed state ($R_0 \simeq 0$) in the thermodynamic limit $N \to \infty$, the value of $R(0)$ should be zero (or negligibly small) at $t = 0$. The scaling law for τ_2 is expected to be N^2 if $\eta_{\text{eff}} \simeq \eta_0 N$.

However, for an ideal chain model with a fixed bond length, such as the freely-jointed chain model, a proposed expression for the free energy is given by $F \sim k_{\mathrm{B}}T\left[\frac{N\ell^2}{R^2} + \frac{R^2}{N\ell^2}\right]$[24,49]. Using this free energy, the time evolution of R take the same form as Eq. (3). Additionally, the final chain size also follows the required scaling behavior of $R_f \sim \ell N^{1/2}$. The characteristic time τ_2 scales similarly as N^2, but the exponent α_2 becomes smaller, namely $\frac{1}{4}$.

In the following sections, we will perform molecular dynamics simulations to evaluate which form of the free energy is more appropriate for describing the expansion behavior in this stage.

Model and setup

We perform computer simulations in d-dimensional space to verify the theory, using the freely-jointed chain (FJC) model. A simulated chain consists of N segments, connecting $N+1$ point monomers. Each segment has an equilibrium length ℓ and is modeled by a harmonic potential given by $U_i = \frac{1}{2}k_{\rm sp}\left(|\boldsymbol{r}_{i-1}-\boldsymbol{r}_i|-\ell\right)^2$ where $k_{\rm sp}$ is the spring constant, and $\boldsymbol{r}_{i-1}$ and $\boldsymbol{r}_i$ are the positions of the adjacent monomers. The dynamics of the chain are described by a system of Langevin equations:

$$m\frac{{\rm d}^2\boldsymbol{r}_i}{{\rm d}t^2} = -\eta_0\frac{{\rm d}\boldsymbol{r}_i}{{\rm d}t} - \frac{\partial U_{\rm tot}}{\partial \boldsymbol{r}_i} + \boldsymbol{\xi}_i \tag{4}$$

for the monomers $i = 0, \ldots, N$, where m denotes the mass of a monomer, η_0 is the friction coefficient of particle, $U_{\rm tot} = \sum_{j=1}^{N} U_j$ is the total potential energy, and $\boldsymbol{\xi}_i$ is the white noise satisfying $\langle\boldsymbol{\xi}_i(t)\rangle = \boldsymbol{0}$ and $\langle\boldsymbol{\xi}_i(t)\cdot\boldsymbol{\xi}_j(t')\rangle = 2dk_{\rm B}T\eta_0\delta_{ij}\delta(t-t')$ with T denoting the temperature.

The negative gradient $-\frac{\partial U_{\rm tot}}{\partial \boldsymbol{r}_i}$ represents the spring forces acting on the monomer i, which is given by $-k_{\rm sp}\left(|\boldsymbol{r}_i-\boldsymbol{r}_{i-1}|-\ell\right)\frac{\boldsymbol{r}_i-\boldsymbol{r}_{i-1}}{|\boldsymbol{r}_i-\boldsymbol{r}_{i-1}|} - k_{\rm sp}\left(|\boldsymbol{r}_i-\boldsymbol{r}_{i+1}|-\ell\right)\frac{\boldsymbol{r}_i-\boldsymbol{r}_{i+1}}{|\boldsymbol{r}_i-\boldsymbol{r}_{i+1}|}$ for $i = 1, \ldots, N-1$. If $i = 0$ or N, the negative gradient includes only one spring force, which is, respectively, the second and the first term in the above expression. The temperature T represents the theta temperature. At this specific temperature, the interactions between monomers are canceled out by the interactions with the solvent molecules. Therefore, the chain behaves like an ideal chain and there are no non-bonded interactions between monomers in the model. This condition is referred to as "the theta condition".

The three quantities, ℓ, m, and $k_{\rm B}T$, are chosen as the basic units for length, mass, and energy, respectively, in the simulations. Therefore, the value of any physical quantity can be expressed using a unit derived directly from these units. For example, the spring constant is set to $k_{\rm sp} = 12{,}000\,k_{\rm B}T/\ell^2$, which is simply denoted as $k_{\rm sp} = 12{,}000$ by omitting the unit "$k_{\rm B}T/\ell^2$". The friction coefficient η_0 is set to 20.0 by omitting the unit $\sqrt{mk_{\rm B}T}/\ell$. The equations of motion are solved using the LAMMPS package[50], employing the Verlet algorithm with an integration time step of $\Delta t = 0.005$ (the omitted time unit is $\ell\sqrt{m/k_{\rm B}T}$). Under these settings, the average segment length is found to be 1.00(2), with the error of 0.02 calculated at the 95% confidence level. The small error asserts that the segment length remains approximately constant. Thus, the model aligns well with the framework of a FJC model.

We initially confine a chain in a small cavity of diameter D. The shape of the cavity is a sphere in 3-dimensional space and a circle in 2-dimensional space. The cavity walls reflect the monomer points inward, thus enclosing the entire chain. After the confined chain reaches an equilibrium state, the cavity walls are suddenly switched off, and the chain undergoes an expansion process from a globule state to a final coil state. We perform 1000 independent runs for each confining condition and chain length to investigate the kinetic behavior of the expansion. In this study, we vary the chain length from $N = 32$ to $N = 512$. The chain length can be described using the exponent g_N, which relates to the chain length through the equation $N = 2^{g_N}$. The diameter of the cavity can also be defined by the diameter exponent g_D through the relation $D = 2^{g_D}$. The value of g_D varies from 1 to 3. The advantage of using g_N and g_D is that it allows us to study the scaling behavior of the expansion kinetics in a clear and systematic manner.

Snapshots of simulation for $N = 512$ and $D = 2.0$ are provided in Fig. 1. Initially, the chain is confined inside a spherical cavity in 3D space (see Picture (a1)) and inside a circular disk in 2D space (see Picture (b1)). As the process begins, the chain expands while maintaining a globule state with a spherical conformation in Picture (a2) and a disklike one in Picture (b2). The chain conformation gradually changes to a coil-like shape with the evolution of time, as shown in Pictures (a3) and (b3) for the space dimension $d = 3$ and $d = 2$, respectively.

Movies illustrating the expansion of a chain in the two spaces can be found in the Supporting Information (SI).

Results

Evolution of chain size

The kinetic of the system is studied by calculating the averaged time variation of chain size, defined by $R(t) = \left\langle R_{\rm g}^2(t)\right\rangle^{1/2}$ where

$$R_{\rm g}^2(t) = \frac{1}{N+1}\sum_{i=0}^{N}\left(\boldsymbol{r}_i(t)-\boldsymbol{r}_{\rm cm}(t)\right)^2 \tag{5}$$

is the square of the radius of gyration of the chain at time t in a run, $\boldsymbol{r}_i(t)$ is the position of the ith monomer, and $\boldsymbol{r}_{\rm cm}(t)$ is the center of mass of the chain. The averaged evolution is obtained from 1000 independent runs for each chain length and confining condition. Figure 2 presents the results of calculation for the cases in (a) 3- and (b) 2-dimensional spaces. Because $N = 2^{g_N}$ and $D = 2^{g_D}$, the number density of segments in the confining cavity is equal to $C_0 = \frac{2d}{\pi}\times 2^{g_N - dg_D}$ in the d-dimensional space.

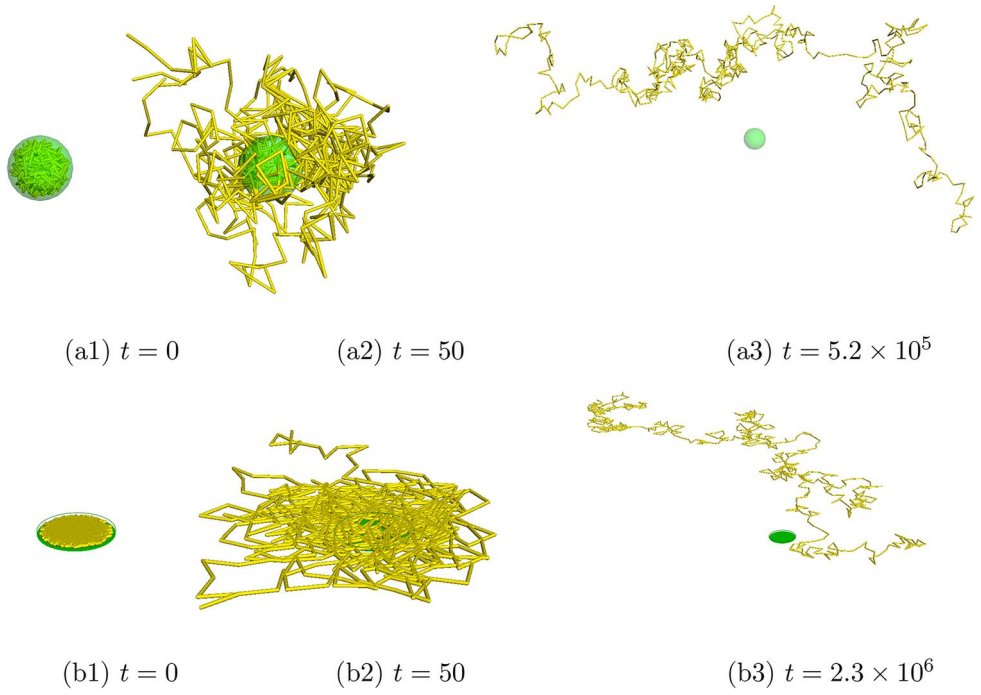

Fig. 1. Snapshots of the simulation for a chain length of $N = 512$ upon release from a cavity with a diameter of $D = 2.0$ are shown in (**a1**–**a3**) for 3D space and in (**b1**–**b3**) for 2D space. The chain is represented by yellow sticks, while the cavity is drawn in green. The moment of time is indicated in the figures. For $t > 0$, the cavity wall has no interaction with the chain and is included in the figure to show the relative size and position of the chain.

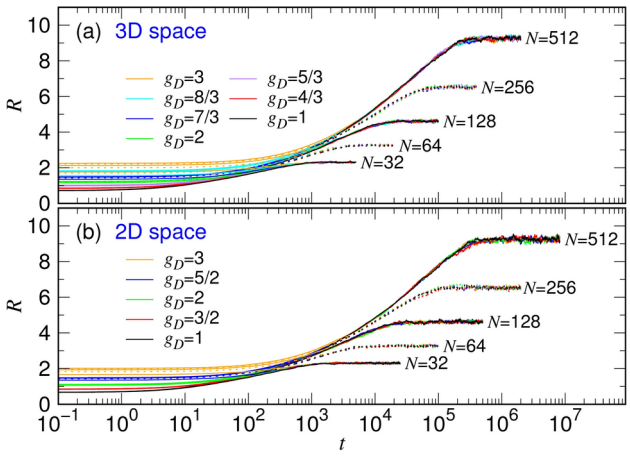

Fig. 2. Averaged time variation of chain size $R(t)$ upon release in (**a**) the 3D space and (**b**) the 2D space. The chain length N is indicated on the right-hand side of the set of the curves. The g_D value can be read from the legends.

We can see that the chain size exhibits sigmoidal variation on the plot of logarithmic time scale. The initial chain size R_0 is mainly determined by the cavity diameter, or the g_D value. It is not sensitive to the chain length N. The final chain size R_f, on the other hand, is determined by N (or the g_N value) and not dependent on D (or g_D). Therefore, the kinetic curves upon releasing from different g_D merge together eventually for the cases with the same N.

It is worth noticing that the size variation during an expansion displays significant fluctuations across individual runs, making it impossible to assess the progress of the process based solely on a single run. Figure S2 in SI illustrates the fluctuations using $N = 128$ released from the condition of $g_D = 1$, with data plotted on

both linear and logarithmic time scales. The results are compared to the averaged variation curves, which are represented by thick green lines.

The total simulation time varies for the studied cases, as can be seen in Fig. 2. An explanation of how we determine the simulation time is provided in Section S3 of SI.

In this study, a logarithmic scale is employed in a figure for the two main situations: (1) to visualize the detailed variation of a quantity whose values span several orders of magnitude on the scale, and (2) to demonstrate the presence of some scaling behavior of a quantity along the scale.

The mean size R_0 of the chain in the cavity and the equilibrium size R_f of the released chain after reaching a natural state in the solution are studied and plotted in Fig. 3 as a function of chain length N.

The value of R_0 is approximately constant for a given g_D. However, slight increase with N can be observed. It suggests that the monomers distribute more closely to the wall than to the cavity center, particularly as N becomes large. Comparing to a globule formed in poor solvent, the outer layer is expected to have a lower monomer density than the center[30,31].

The final chain size R_f is independent of the initial confining condition. It scales with N as $R_f \sim N^{0.501(2)}$ in the 3D space and as $R_f \sim N^{0.500(2)}$ in the 2D space, consistent with the well-known $N^{1/2}$ behavior for a random walk. Noticeably, the obtained 3D value for R_f is identical to the 2D value at a given N. It is because the lengths of a step in the 3D and in the 2D random walk are identical. Both of them are equal to the segment length ℓ.

Variation of chain shape

To understand how the chain conformation changes during an expansion process, we calculated the asphericity in d-dimensional space, defined by

$$A_d(t) = \left\langle \frac{\sigma_\lambda^2}{d\bar{\lambda}^2} \right\rangle \tag{6}$$

where $\bar{\lambda} = \frac{1}{d}\sum_{\alpha=1}^{d} \lambda_\alpha$ is the mean of the eigenvalues λ_α (for $\alpha = 1, \ldots, d$) of the gyration tensor $\boldsymbol{Q}$ of the chain at time t, and $\sigma_\lambda^2 = \frac{1}{d-1}\sum_{\alpha=1}^{d}(\lambda_\alpha - \bar{\lambda})^2$ is the variance[51]. The components of $\boldsymbol{Q}$ are computed by

$$Q_{\alpha\beta} = \frac{1}{N+1}\sum_{i=0}^{N}(r_{i,\alpha}(t) - r_{\mathrm{cm},\alpha}(t))(r_{i,\beta}(t) - r_{\mathrm{cm},\beta}(t)). \tag{7}$$

Since the numerator in A_d represents the variance of the eigenvalues, the asphericity measures how much the chain shape deviates from spherical symmetry, taking a value between 0 (no deviation from a sphere) and 1 (largest deviation with a rod-like shape) after the suitable normalization in the denominator. The ensemble average $\langle\cdot\rangle$ in Eq. (6) is calculated over 1000 independent runs for each studied case at each time stamp. The results are presented in Fig. 4.

For each chain length N, expansions released from different confining conditions, with g_D varying from 1 to 3, are studied and plotted using lines of the same color scheme. A stronger confinement results in a more sphere-like initial chain structure, leading to a smaller value of A_d. As a result, the curve is positioned lower for smaller g_D. Therefore, these lines in the small time region are distinguishable. An example is provided for $N = 32$,

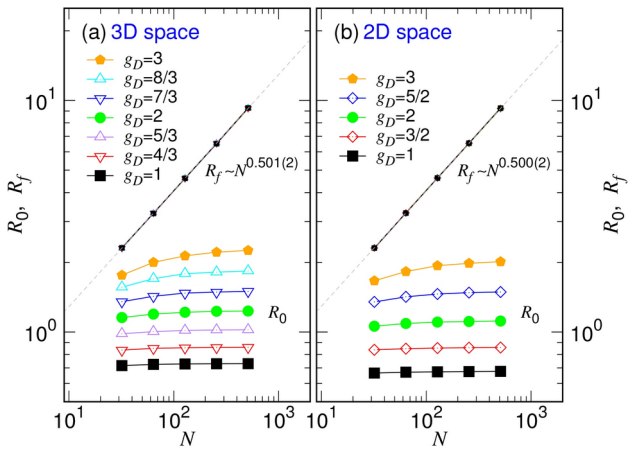

Fig. 3. Initial chain size R_0 (represented by large symbols) and final equilibrium size R_f of the chain after release (represented by small symbols) are plotted as a function of N in (**a**) the 3D space and (**b**) the 2D space. The value of g_D are indicated in the legend.

where the g_D value is printed on top of the corresponding orange curve, shown on the left side of the figure, in increasing order from the bottom to the top.

We found that for a long chain, such as $N = 512$, the A_3 curves for the 3D expansion are very close to zero and increase slowly at the beginning. It indicates that the chain undergoes a spherical expansion initially, known as globule expansion. As time passes, the chain shape evolves rapidly and deviates from a spherical form, resulting in a significantly increased A_3. For different g_D values, the A_3 curves eventually merge and follow a principal route of evolution, tending toward a final value of 0.394(7). This final value is consistent with the value published in literature[51–53] for a Gaussian coil. Consequently, in the second stage of expansion, the chain adopts a coil structure. A similar behavior is observed in the 2D expansion: the A_2 value is initially about zero for a long chain and evolves to reach a coil value of 0.395(9).

This study demonstrates that the chain structure transitions from a globule state to a coil state during the expansion.

Time scaling of $\tilde{R}_1$ and $\tilde{R}_2$

In order to analyze the scaling properties of the chain size in detail, the two dimensionless quantities are investigated: $\tilde{R}_1 = R/R_0$ and $\tilde{R}_2 = R/R_f$. The first quantity measures the ratio of the chain's expansion relative to its initial size, while the second indicates the percentage of recovery during the expansion as it approaches the final, natural size of the chain in a bulk solution. The results are presented in Fig. 5 for both 3D and 2D spaces.

We can observe in Panels (a1) and (b1) that the $\tilde{R}_1$ curves for different values of N collapse at the same g_D value in the small time region, indicating that the expansion kinetics are determined by the initial confining conditions. In Panels (a2) and (b2), the $\tilde{R}_2$ curves overlap in the large time region for a given N, providing further evidence that the kinetics for different g_D values follow the same recovery path as $\tilde{R}_2$ approaches 1. The sigmoidal variations suggest that the process undergoes a two-stage expansion, with each stage having its own characteristic time of expansion.

The collapsed and merged curves exhibit similarity and regularity on the semilog plot, suggesting the presence of a scaling property for the characteristic times. To test the idea, the time is multiplied by specific scaling factors to horizontally shift the curves. For the $\tilde{R}_1$ curves, the time is scaled using the formula $t_{\omega_1} = t \times \omega_1^{-d(g_D - g_{D,0})}$, where ω_1 is a parameter to be determined. An optimal choice of ω_1 should result in the collapse of all curves onto the target curve corresponding to $D = 2^{g_{D,0}}$ in the first stage. We selected $g_{D,0} = 1$. The best collapse is achieved by varying ω_1 to minimize the width of the set of shifted curves within a specific t_{ω_1} region. We found that $\omega_1 = 1.98$ for the 3D expansion and $\omega_1 = 2.79$ for the 2D expansion yield the best collapse of the curves in the small time region $t_{\omega_1} < 10$, as illustrated in Panels (a1) and (b1) of Fig. 6.

Similarly, the $\tilde{R}_2$ curves can be merged in the second stage by shifting the curves using the scaled time $t_{\omega_2} = t \times \omega_2^{-(g_N - g_{N,0})}$. We selected $g_{N,0} = 9$ and found that $\omega_2 = 4.04$ for the 3D expansion and $\omega_2 = 4.03$ for the 2D expansion produce the best merging of the curves in the region $t_{\omega_2} > 5 \times 10^4$. Illustrations can be found in Panels (a2) and (b2) of Fig. 6. A detailed explanation of how we obtained the optimal values for ω_1 and ω_2 is provided in SI, along with Fig. S3. Figure S4 demonstrates that the width of the collapse increases when we choose ω_1 and ω_2 values that deviate from the optimal ones.

The collapsed variations in the first stage of expansion are fitted using the nondimensionalized Eq. (2)

$$\tilde{R}_1(t) = \left(1 + \frac{t}{\tau_1}\right)^{\alpha_1} \tag{8}$$

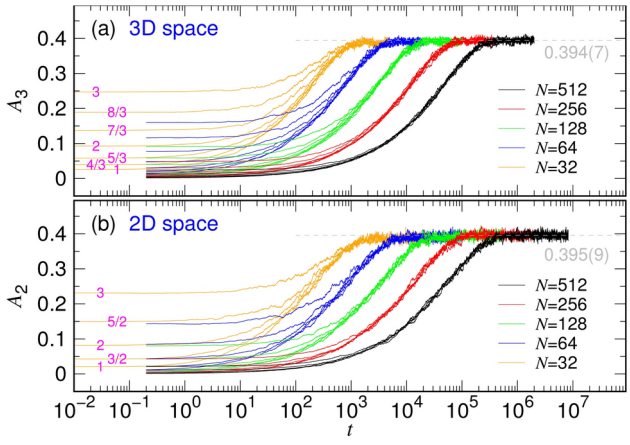

Fig. 4. Time evolution of the asphericity A_d for the expansion process in (**a**) 3D space and (**b**) 2D space. The color scheme for chain length N is indicated in the legend. The confining condition, defined by g_D, is provided for $N = 32$ case, presented as an example, where the value is printed directly on top of the corresponding curve on the left side of the figure. The same value and order of g_D apply to the other chain lengths.

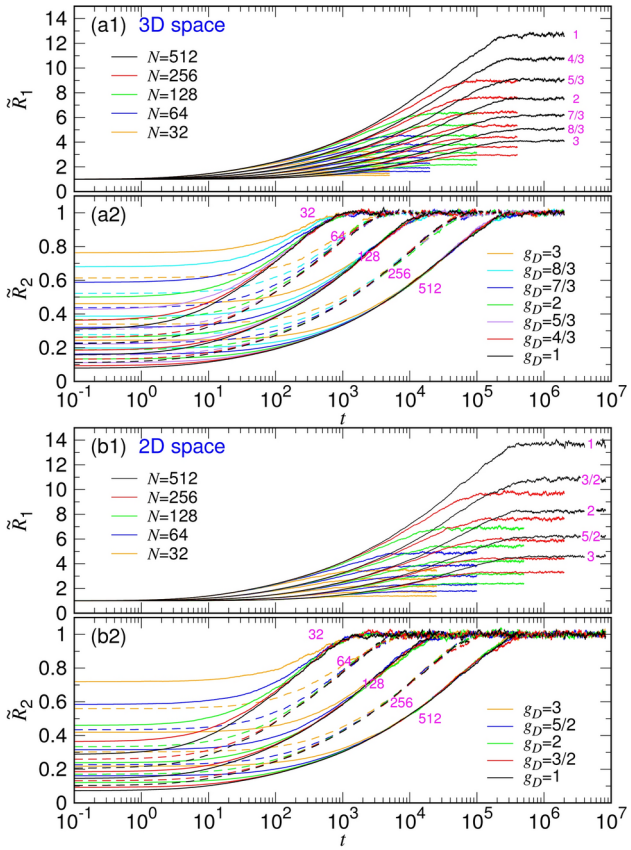

Fig. 5. Time evolution of $\tilde{R}_1 = \frac{R}{R_0}$ and $\tilde{R}_2 = \frac{R}{R_f}$ shown in Panels (**a1**, **a2**) for the 3D space and (**b1**, **b2**) for the 2D space. In the plots of (**a1**) and (**b1**), the chain length N is indicated in the legend. For each N, several confining conditions are studied, defined by the g_D values. The smaller the g_D value, the higher the $\tilde{R}_1$ curve. On the right side of the curves for $N = 512$, the g_D values are printed as an example. The same order of curves applies for these g_D values across the other chain lengths. In the plots of (**a2**) and (**b2**), N is indicated above the merged curves, and the g_D value can be found in the legend.

through a two-parameter fit. The obtained results are $(\tau_1, \alpha_1) = (3.62(8), 0.293(5))$ for the 3D expansion and (5.85(9), 0.338(4)) for the 2D expansion. The fitting curves are plotted in Fig. 6a1, b1 as magenta dashed lines, which fit to the data in the small time region but eventually become divergent as time increases. Consequently, in the large time region, the curves should be fitted using the dimensionless version of Eq. (3),

$$\tilde{R}_2(t) = \left(1 - \exp\left(-\frac{t}{\tau_2}\right)\right)^{\alpha_2}. \tag{9}$$

We obtained $(\tau_2, \alpha_2) = (9.39(7) \times 10^4, 0.258(2))$ and $(1.47(1) \times 10^5, 0.242(2))$ for the 3D and 2D expansion, respectively. The fitting curves, displayed also in magenta dashed lines in Panels (a2) and (b2), fit the data well in the time region and tend toward the finial value 1 as expected.

The collapse study presented here enables a deeper analysis of scaling behaviors. For instance, the optimized value of ω_1 suggests that τ_1 should scale as D^{x_1}, with the exponent $x_1 = d \log_2 \omega_1$, assuming $R_0 \sim D$. The obtained values of $\omega_1 = 1.98$ and 2.79 for the two spatial dimensions correspond to $x_1 = 2.957$ and 2.961, respectively. Since our theory predicts $x_1 = \frac{1}{\alpha_1}$ with $\alpha_1 = 2 + \frac{1}{\nu} + y_1$, these results further suggest that the exponent y_1, introduced for $\eta_{\text{eff}} \sim \eta_0 N \left(\frac{R}{\ell}\right)^{y_1}$, should be approximately -1. Similarly, based on the optimized values of ω_2, which are 4.04 and 4.03 for the two spatial dimensions, we can calculate the exponent $x_2 = \log_2 \omega_2$ for the scaling relation $\tau_2 \sim N^{x_2}$. The obtained x_2 values are 2.014 and 2.011, respectively, which align well with the theoretical prediction of $x_2 = 2$.

Characteristic times τ_1 and τ_2 and exponents α_1 and α_2

The characteristic times and exponents can be further investigated by fitting the single $\tilde{R}_1(t)$ and $\tilde{R}_2(t)$ curves for each case, using Eq. (8) and Eq. (9) respectively. The goodness of the fit is illustrated in Fig. S5 of SI. The reason why the parameter C in Eq. (3) can be set to one is explained in SI, along with Fig. S6.

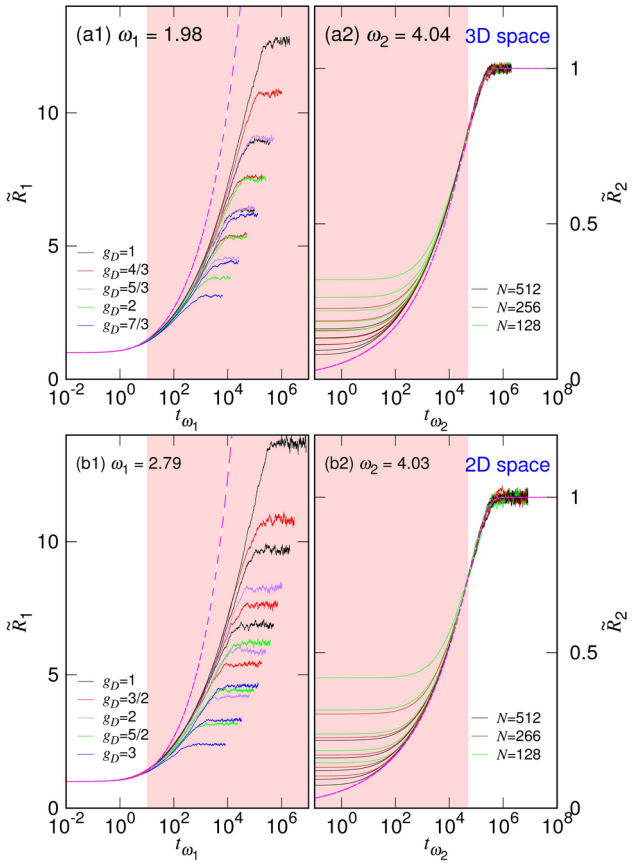

Fig. 6. Collapse study of (**a1**, **b1**) the $\tilde{R}_1$ curves and (**a2**, **b2**) the $\tilde{R}_2$ curves in the 3D and 2D spaces. The scaled time are defined as $t_{\omega_1} = t \times \omega_1^{-d(g_D - g_{D,0})}$ and $t_{\omega_2} = t \times \omega_2^{-(g_N - g_{N,0})}$, with $g_{D,0} = 1$ and $g_{N,0} = 9$. The best collapse of $\tilde{R}_1$ is achieved using $\omega_1 = 1.98$ for the 3D apace and 2.79 for the 2D spaces. The best collapse for $\tilde{R}_2$ is obtained with $\omega_2 = 4.04$ and 4.03, respectively. The magenta dashed lines represent the fitting curves obtained from Eqs. (8) and (9) for the first and second stages of expansion.

The obtained values of τ_1 and τ_2 for the 3D and 2D spaces are presented in Fig. 7. Panels (a1.1) and (b1.1) show that τ_1 remains approximately constant and is not sensitive to variations in N at a given g_D. The plots in Panels (a1.2) and (b1.2) further reveal that the characteristic time increases with the initial chain size R_0, with a power-law exponent equal to 3.2(2) for 3D space and 3.1(2) for 2D space. The results indicate that τ_1 scales approximately as $N^0 R_0^3$, consistent with the findings from the collapse study of the $\tilde{R}_1(t)$ curves in the previous subsection.

Panels (a2.1), (a2.2), (b2.1), and (b2.2) indicate that the characteristic time for the second expansion stage increases with N, with exponents of 1.98(4) and 2.00(6) for the two spatial dimensions. The suggested scaling relation is $\tau_2 \sim N^2 D^0$, consistent also with the collapse study of the $\tilde{R}_2$ curves.

The exponents α_1 and α_2 obtained from the fitting analysis are displayed in Fig. 8. For a confinement with small D, such as in the case of $g_D = 1$, α_1 attends a value of approximately 0.33 in the plots of Panels (a1.1) and (b1.1), while α_2 is around 0.24 in Panels (a2.1) and (b2.1) for the 3D and 2D expansions. As the degree of confinement decreases, or equivalently, as the cavity diameter D increases, the value of α_1 decreases (see Panels (a1.2) and (b1.2)). A similar trend can be seen for α_2 in Panels (a2.2) and (b2.2); however, the rate of decrease is suppressed as N increases, particularly in the cases of $N = 256$ and 512.

Generally speaking, in the limit of strong confinement for a long chain, the two exponents approach asymptotic values of approximately $\frac{1}{3}$ and $\frac{1}{4}$, respectively, regardless of the spatial dimension. To verify the observations, we plot the quantity

$$\Theta_{\alpha_1} = \frac{t}{\tilde{R}_1^{1/\alpha_1} - 1} \tag{10}$$

as a function of $\tilde{R}_1$. A suitable choice of α_1 should yield a constant function during the first expansion stage, with the value equal to τ_1. Figure 9 presents the results of calculation using three test values: $\alpha_1 = \frac{1}{2}, \frac{1}{3}$, and $\frac{1}{4}$, for the case of $N = 512$ and $g_D = 1$. We can see that $\alpha_1 = \frac{1}{3}$ yields the best result in the region of $\tilde{R}_1 < 1.4$, with a constant value of 4.54 for 3D space and 5.75 for 2D space, which is consistent with the fitting obtained in Fig. 7.

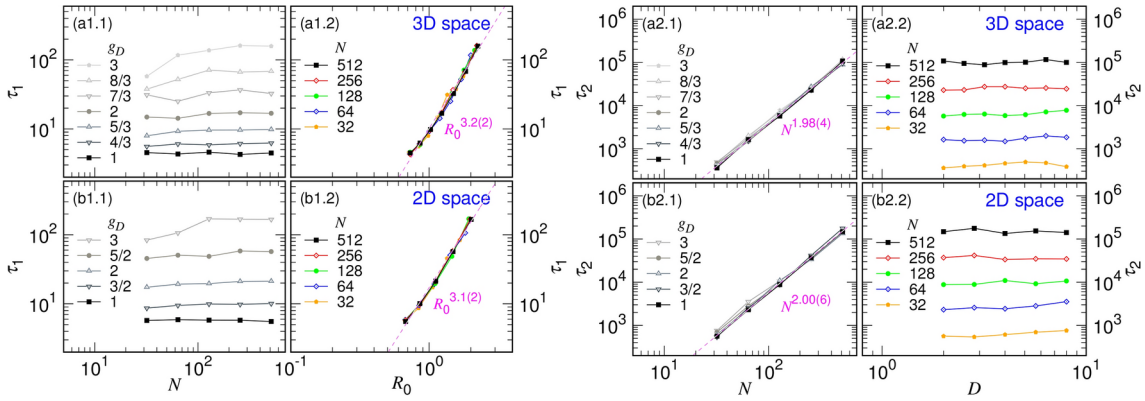

Fig. 7. Characteristic time τ_1 in the first expansion stage plotted against N for various values of g_D (as indicated in the legend) in (**a1.1**) for 3D space and (**b1.1**) for 2D space. Additionally, τ_1 is studied against the initial chain size R_0 for different values of N (which can also be found in the legend) in (**a1.2**) for 3D and (**b1.2**) for 2D spaces. Similarly, the characteristic time τ_2 for the second expansion stage is presented against N in (**a2.1**) and (**b2.1**). τ_2 versus the diameter D of the confining cavity is shown in (**a2.2**) and (**b2.2**) for various chain lengths.

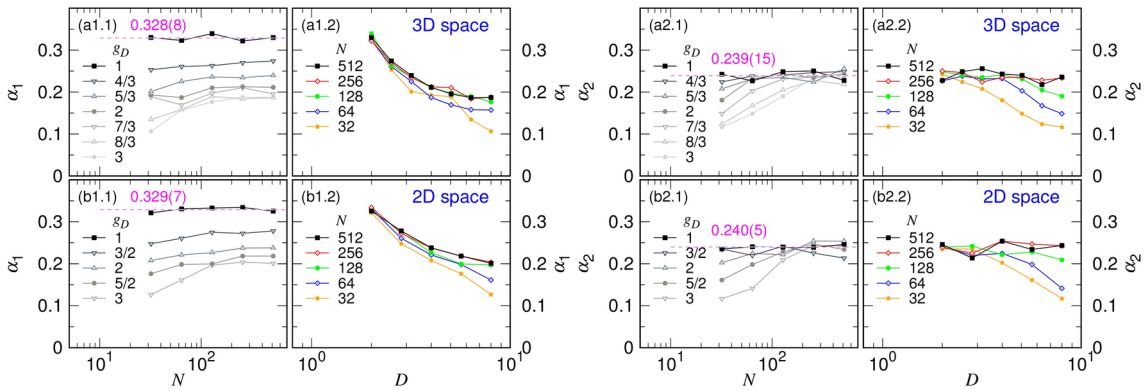

Fig. 8. Exponent α_1 in the first expansion stage plotted against N for various values of g_D (as indicated in the legend) in (**a1.1**) for 3D space and (**b1.1**) for 2D space. Additionally, α_1 is analyzed against the cavity diameter D for different values of N (which can also be found in the legend) in (**a1.2**) for 3D and (**b1.2**) for 2D spaces. Similarly, the exponent α_2 for the second expansion stage is presented against N in (**a2.1**) and (**b2.1**). α_2 versus D for various N is shown in (**a2.2**) and (**b2.2**) for the two spaces.

To evaluate the α_2 value, we plot the quantity

$$\Xi_{\alpha_2} = \frac{\alpha_2 \left[\tilde{R}_2^{1-\frac{1}{\alpha_2}} - \tilde{R}_2\right]}{\frac{d\tilde{R}_2}{dt}} \tag{11}$$

as a function of the recovery percentage $\tilde{R}_2$, which is expected to be constant during the second stage of expansion. The scaled expansion speed $\frac{d\tilde{R}_2}{dt}$ in the denominator is calculated by taking the time derivatives of $R_g(t)$ from individual runs and then computing the ensemble average, normalized by R_f. The results obtained using the test values $\alpha_2 = \frac{1}{2}, \frac{1}{3}, \frac{1}{4}$, and $\frac{1}{5}$ are presented in Fig. 10.

We found that $\alpha_2 = \frac{1}{4}$ produces the best constant variation behavior in the region $\tilde{R}_2 > 0.6$, despite the presence of fluctuation noise. The constant value is approximately 9.65×10^4 for the 3D expansion and 1.53×10^5 for the 2D expansion, which aligns well with the fitting τ_2 given in Fig. 7 for the case of $(N, g_D) = (512, 1)$.

Since the expansion is divided into the two stages, the time interval representing each stage can be described by its own characteristic time: from the beginning up to a few τ_1 for the first stage, and starting at some fraction

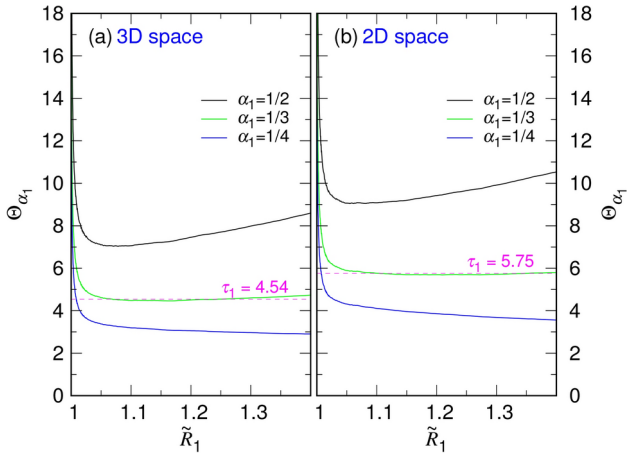

Fig. 9. Physical quantity Θ_{α_1}, calculated by Eq. (10) at the three α_1 values given in the legend, is plotted against $\tilde{R}_1$ for (**a**) 3D space and (**b**) 2D space.

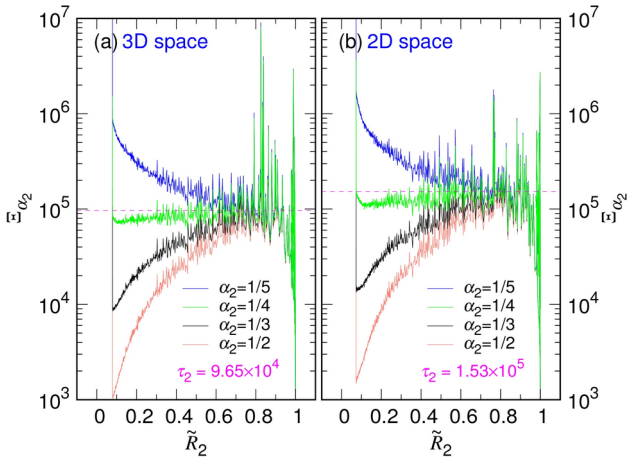

Fig. 10. Physical quantity Ξ_{α_2}, calculated by Eq. (11) at the four α_2 values given in the legend, is plotted against $\tilde{R}_2$ for (**a**) 3D space and (**b**) 2D space.

of τ_2 until the end of the simulations for the second stage. In this study, we fit τ_1 from the size variation data with $\tilde{R}_1 < 1.4$ and fit τ_2 with $\tilde{R}_2 > 0.6$. Thus, the corresponding time intervals can be considered as $t < 1.74\tau_1$ and $t > 0.139\tau_2$, respectively.

We emphasize that the theory developed here is phenomenological, describing the kinetic evolution of chain size in an approximate manner. There is no precise definition for delineating the intervals, as the chain gradually changes its conformation from a sphere to a coil, as shown in Fig. 4 for the variation of asphericity. Furthermore, due to the large fluctuations observed in Fig. S2 of SI, it is not feasible to determine the intervals through a single run. The estimated intervals provided in the previous paragraph should be regarded merely as a guideline for the averaged expansion behavior.

Expansion speed

The speed of expansion, $\frac{dR}{dt}$, is analyzed by calculating the average time derivatives of $R_g(t)$ from individual runs. The results are presented in Fig. 11.

Panels (a1) and (b1) show the time variations of speed for $N = 512$ released from different confining conditions in 3D and 2D spaces, while Panels (a2) and (b2) display the variations for $g_D = 1$ as the chain length changes. We observed that the speed initially surges from zero and reaches a peak in the logarithmic time scale. The height of the peak decreases as the confinement becomes looser, although the peak position occurs at roughly the same moment after release. For $g_D = 1$, the variations in speed are surprisingly not sensitive to the chain length due to the lack of interaction between monomer points. The driving force behind the expansion is purely entropic. Consequently, the speed profiles during the process are similar and collapse together, as illustrated in the figure.

The magenta dashed lines in Panels (a1) and (b1) represent the predicted speed, given by

$$\frac{\mathrm{d}R}{\mathrm{d}t} = \frac{\alpha_1 R_0}{\tau_1}\left(1+\frac{t}{\tau_1}\right)^{\alpha_1-1}. \tag{12}$$

In this equation, the values of τ_1 and α_1 are taken from the fitting results in Figs. 7 and 8. We can see that the equation aligns quite well with the speed variation in the first stage. However, it fails to describe the transient behavior immediately after the chain is elapsed from a confined state (where the speed is zero).

The expansion speed in the second stage is well described by the equation

$$\frac{\mathrm{d}R}{\mathrm{d}t} = \frac{\alpha_2 R_f}{\tau_2}\left(1-\exp\left(-\frac{t}{\tau_2}\right)\right)^{\alpha_2-1}\exp\left(-\frac{t}{\tau_2}\right), \tag{13}$$

as depicted by the magenta dashed lines in Panels (a2) and (b2) for the 3D and 2D spaces, respectively. Likewise, the parameters τ_2 and α_2 are sourced from Figs. 7 and 8.

The speed given by Eq. (12) for the first stage indicates that $\frac{\mathrm{d}R}{\mathrm{d}t}$ should depend solely on the confining condition, and not on the chain length. It is because the leading factor $\frac{\alpha_1 R_0}{\tau_1}$ has no chain length dependence. Since $\tau_1 \sim R_0^3$ and R_0 is primarily proportional to the cavity diameter D, an identical speed profile is predicted, as observed in the time region $t < 10^2$ of Panels (a2) and (b2) for different N values at $g_D = 1$. In contrast, Eq. (13) predicts an N-dependent speed profile for the second expansion stage, because $R_f \sim N^{1/2}$ and $\tau_2 \sim N^2$, which are independent of the confining condition.

The simulations confirm these predicted behaviors. To illustrate it, Fig. 11 is replotted in Fig. S7 using a log-log scale, which allows for a detailed view of the small speeds. In the large time region, we observe the merging of speed profiles for $N = 512$ at various g_D in Panels (a1) and (b1). Conversely, for the given $g_D = 1$ across different N values, the curves collapse in the small time region and become separated as time increases, as shown in Panels (a2) and (b2).

Kinetic equations

Our theory predicts two kinetic equations for the corresponding expansion stages:

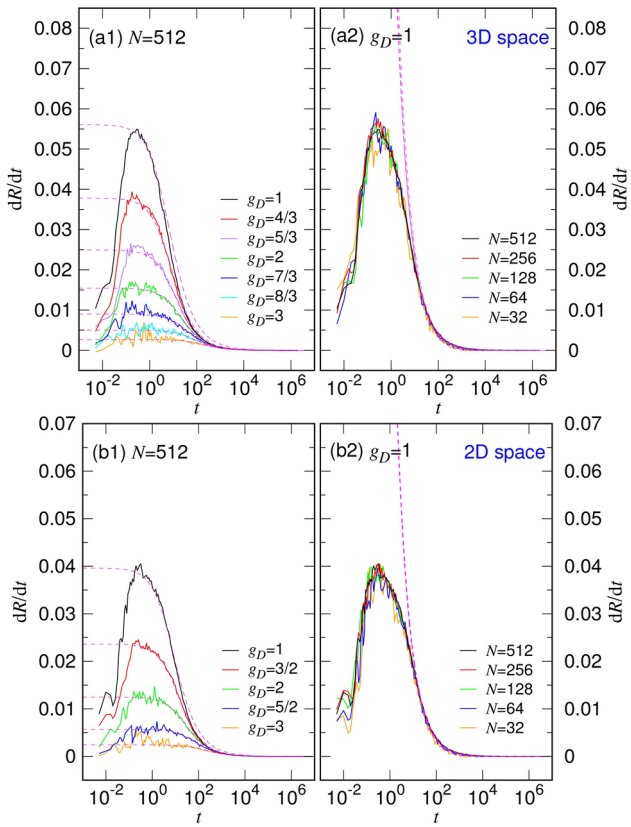

Fig. 11. Expansion speed $\mathrm{d}R/\mathrm{d}t$ in 3D space plotted as a function of time t: (**a1**) at a fixed chain length $N = 512$ for various values of g_D, and (**a2**) at $g_D = 1$ for different N cases. Similar plots of $\mathrm{d}R/\mathrm{d}t$ versus t in 2D space are shown: (**b1**) at a fixed $N = 512$ for various g_D values, and (**b2**) at $g_D = 1$ for different N.

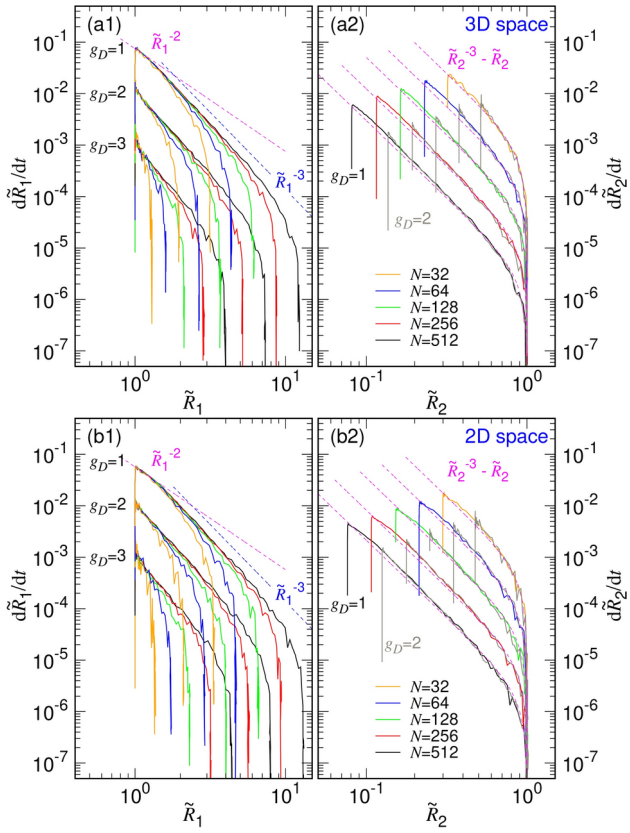

Fig. 12. $\frac{\mathrm{d}\tilde{R}_1}{\mathrm{d}t}$ vs. $\tilde{R}_1$ in (**a1**) the 3D and (**b1**) the 2D spaces. The color codes for N can be found in the legends. Three g_D values are presented, indicated on the left side of the set of the curves. The curves of $\frac{\mathrm{d}\tilde{R}_2}{\mathrm{d}t}$ vs. $\tilde{R}_2$ are presented in (**a2**) for 3D space and (**b2**) for 2D space. The colored curves (including the black one) represent the cases run at $g_D = 1$ for different N. The gray curves, which overlay the colored ones, are the ones conducted at $g_D = 2$.

$$\frac{\mathrm{d}\tilde{R}_1}{\mathrm{d}t} = \frac{\alpha_1}{\tau_1}\tilde{R}_1^{1-\frac{1}{\alpha_1}}, \tag{14}$$

$$\frac{\mathrm{d}\tilde{R}_2}{\mathrm{d}t} = \frac{\alpha_2}{\tau_2}\left[\tilde{R}_2^{1-\frac{1}{\alpha_2}} - \tilde{R}_2\right], \tag{15}$$

which are the ordinary differential equations that yield the solutions of Eqs. (8) and (9), respectively. Simulations provide a unique opportunity to verify these kinetic equations in a direct way by plotting $\frac{d\tilde{R}_1}{dt}$ versus $\tilde{R}_1$ and $\frac{d\tilde{R}_2}{dt}$ versus $\tilde{R}_2$. The results are presented in Fig. 12 for the two spatial dimensions.

In Panels (a1) and (b1), we can see that the evolution curves, starting from $\tilde{R}_1 = 1$, overlap at a given g_D value for different chain lengths. This suggests that the initial expansion behavior is determined by the confining conditions rather than the chain length. For the case elapsed from the strong confinement $g_D = 1$, the expansion speed $\frac{d\tilde{R}_1}{dt}$ exhibits a scaling behavior of $\tilde{R}_1^{-2}$, as indicated by the magenta dashed line. It confirms that α_1 should be $\frac{1}{3}$ in the two spaces.

The slope of the curves then decreases rapidly, exhibiting a kink, and maintains at approximately -3 (as shown by the blue dashed line) for a long duration. Near the end of the expansion, the curves drop sharply because the speed approaches zero. The behaviors are further analyzed in Panels (a2) and (b2), where $\frac{d\tilde{R}_2}{dt}$ is fitted to the predicted second-stage relation $\tilde{R}_2^{-3} - \tilde{R}_2$. The goodness of the fit is illustrated by the magenta dashed lines for N varying from 32 to 512 at $g_D = 1$, reinforcing the finding $\alpha_2 = \frac{1}{4}$.

Moreover, the curves are plotted in the same panels in gray lines for the cases studied with $g_D = 2$. These curves overlap with the colored ones for $g_D = 1$, indicating again that the kinetic evolution is determined by N and not by g_D. Therefore, the speed curves for different g_D coincide on the same recovery path across different chain lengths in the second expansion stage.

Scaling form of free energy

The free energy during the two expansion stages can be analyzed by integrating Eq. (1) as follows

$$F = \int -\eta_{\text{eff}} \left(\frac{\mathrm{d}R}{\mathrm{d}t}\right) \mathrm{d}R. \tag{16}$$

As discussed in section "Theory", η_{eff} denotes the effective chain friction coefficient associated with the state variable $\frac{\mathrm{d}R}{\mathrm{d}t}$, meaning it can depend on the other state variable R and change during the course of the expansion. We hypothesize that η_{eff} adopts the scaling forms of $\eta_0 N \left(\frac{R}{\ell}\right)^{y_1}$ and $\eta_0 N \left(\frac{R}{\ell}\right)^{y_2}$ in the two respective expansion stages. Utilizing the kinetic equation in Eq. (14), we can determine the free energy for the first expansion stage to be

$$F_1(R) = \frac{\alpha_1}{\tau_1} \eta_0 \ell^2 N \frac{1}{\frac{1}{\alpha_1} - 2 - y_1} \left(\frac{R_0}{\ell}\right)^{\frac{1}{\alpha_1}} \left(\frac{R}{\ell}\right)^{-\left(\frac{1}{\alpha_1} - 2 - y_1\right)}. \tag{17}$$

Blob theory predicts the free energy for a globular ideal chain as $F \sim k_{\text{B}} T N (\frac{R}{\ell})^{-1/\nu}$ with $\nu = \frac{1}{2}$. Comparing the two free energies leads to the relationships $\alpha_1 = (2 + \frac{1}{\nu} + y_1)^{-1}$ and $\tau_1 \sim \frac{\eta_0 \ell^2}{kT} \left(\frac{R_0}{\ell}\right)^{\frac{1}{\alpha_1}}$. It implies $y_1 = -1$ because our simulations indicate that $\alpha_1 = \frac{1}{3}$. Figure 7 has demonstrated that τ_1 does scale as R_0^3 in the two spatial dimensions, which reasserts the theoretical framework.

To determine the free energy for the second stage, we substitute Eq. (15) into Eq. (16) and carry out the integration. The result is

$$F_2(R) \simeq \frac{\alpha_2}{\tau_2} \eta_0 \ell^2 N \left[\frac{1}{2 + y_2} \left(\frac{R}{\ell}\right)^{2 + y_2} + \frac{1}{\frac{1}{\alpha_2} - 2 - y_2} \left(\frac{R_f}{\ell}\right)^{\frac{1}{\alpha_2}} \left(\frac{R}{\ell}\right)^{-\left(\frac{1}{\alpha_2} - 2 - y_2\right)}\right]. \tag{18}$$

The Flory free energy for a single chain contains a well-known entropic term, specifically $k_{\text{B}} T \frac{R^2}{N\ell^2}$. This term corresponds to the first term on the right side of the equation and suggests that $y_2 = 0$ and $\tau_2 \sim \frac{\eta_0 \ell^2}{kT} N^2$. We have indeed observed a N^2-scaling for τ_2 in Fig. 7. Given the result of $\alpha_2 = \frac{1}{4}$ and the relation $R_f \sim \ell N^{1/2}$, we propose that the general scaling of the free energy for an ideal coil chain can be expressed as

$$F(R) \sim kT \left[\frac{R^2}{N\ell^2} + \frac{N\ell^2}{R^2}\right]. \tag{19}$$

The second term on the right side appears to be a reminiscent contribution to the free energy, evolved from Eq. (17).

Conclusions and discussions

We have performed computer simulations to investigate the expansion kinetics of a confined polymer under theta conditions. The chain was modeled as a freely-jointed chain, initially packaged in a cavity and expanded upon the sudden removal of the confining constraints in both three-dimensional and two-dimensional spaces. The time evolution of the chain size exhibits a sigmoidal variation on the logarithmic scale of time, suggesting a two-stage transition during the expansion process. In the first "globule expansion" stage, the chain undergoes rapid expansion while maintaining a globular conformation. The process then slows down in the second stage, where the shape of the chain transforms into a coil form, known as the "coil expansion" stage. A kinetic theory was developed within the framework of Onsager's variational principle.

We systematically varied the diameter $D = 2^{g_D}$ of the confining cavity and the chain length N, and studied the similarities in the averaged evolution curves of chain size. Two physical quantities, $\tilde{R}_1 = R/R_0$ and $\tilde{R}_2 = R/R_f$ which represent the expansion ratio and the recovery percentage, respectively, were calculated. The analysis of these curves over a scaled time axis revealed that the characteristic time τ_1 for the first expansion stage scales approximately as D^3, while the characteristic time τ_2 for the second stage exhibits a power-law behavior proportional to N^2. Direct fitting of the data using Eqs. (8) and (9) allowed us to reassert the scaling relations for τ_1 and τ_2, and showed that the exponent α_1 is approximately 1/3 and α_2 is about 1/4 for long chains released from strong confinement. The study of the quantities Θ_{α_1} and Ξ_{α_2}, defined respectively in Eqs. (10) and (11), double-confirmed these findings.

We further investigated $\mathrm{d}R/\mathrm{d}t$ and found that the speed profile displays a sharp peak at the beginning, indicating an explosive expansion. Interestingly, chains that expanded under the same confining conditions (the same g_D value) exhibit identical speed profiles; however, the peak height decreases with increasing g_D. Further study for the kinetic equations revealed that $\mathrm{d}\tilde{R}_1/\mathrm{d}t$ scales as $\tilde{R}_1^{-2}$ in the first stage, while $\mathrm{d}\tilde{R}_2/\mathrm{d}t$ scales as $\tilde{R}_2^{-3} - \tilde{R}_2$ in the second stage. Carrying out the integration in Eq. (16), we were able to conclude

that the free energy of the chain takes the form $F \sim k_{\mathrm{B}}T(N\ell^2/R^2)$ in the initial globule-expansion stage and $F \sim k_{\mathrm{B}}T\left[\frac{R^2}{N\ell^2} + \frac{N\ell^2}{R^2}\right]$ in the latter coil-expansion stage.

Compared to the previous results in good solvents[38,39], several noteworthy contrasts emerge. First, the values of $\alpha_1 = \frac{d\nu_b - 1}{2(d\nu_b - 1) + d}$ and $\alpha_2 = \frac{1}{d+2}$ are predicted for good solvents. In contrast, the two exponents are $\frac{1}{3}$ and $\frac{1}{4}$ under theta conditions, and these values are independent of the spatial dimension d. This indicates that a simple substitution of the random-walk exponent $\nu_b = \frac{1}{2}$ into the formula does not yield the exponents in theta solvents. Second, since an ideal chain has zero excluded volume, the volume fraction plays no role in the theoretical framework. As a result, the predicted characteristic time $\tau_1 \sim (R_0/\ell)^{1/\alpha_1}$ exhibits no dependence on the chain length N under theta conditions. In contrast, in good solvents, τ_1 is determined by both the volume fraction ϕ_0 in the confinement and N. Moreover, while τ_2 scales as $N^{2+\chi_2}$ in good solvents, it scales as N^2 under theta conditions. The presence of excluded volume in good solvents prohibits self-crossing of the chain, resulting in a higher power-law dependence, whereas self-crossing is allowed in the ideal chain model we studied. Third, τ_2 is several orders of magnitude larger than τ_1, particularly for expansions released from strong confinement. Therefore, the duration of expansion is primarily governed by the second characteristic time. Moreover, the expansion in 3D occurs more rapidly than that in 2D. For $N = 512$ in good solvents, we found τ_2 to be approximately 3.9×10^5 and 1.9×10^6 for the 3D and 2D expansion, respectively. Under theta conditions, τ_2 is measured at 1.0×10^5 and 1.5×10^5 for the two spatial dimensions (extracted from Fig. 7). The required expansion time is longer in good solvents than in theta solvents, due to the larger final size of the chain achieved as a result of excluded volume interactions.

We have demonstrated that τ_1 scales as R_0^3 in Fig. 7. The following interpretation is proposed: In the initial stage of expansion, the pressure inside a chain globule can be calculated using $P = -\frac{\partial F}{\partial \mathcal{V}_d} \sim \frac{F}{\mathcal{V}_d}$, which exerts a total force of $f = P\mathcal{A}_d$ on the monomers near the surface, where $\mathcal{V}_d$ and $\mathcal{A}_d$ represent the volume and the surface area of the globule of radius R, respectively. There are approximately $N_s \simeq N\frac{\mathcal{A}_d\ell}{\mathcal{V}_d} \sim \frac{N\ell}{R}$ monomers located near the surface. Consequently, the speed of expansion can be estimated by $u \simeq \frac{f}{\eta_{\mathrm{eff}}} \sim \frac{F}{\eta_0 N\ell}$, where the effective friction coefficient is about $\eta_{\mathrm{eff}} \sim \eta_0 N_s$. Thus, the characteristic time is given by $\tau_1 \simeq \int_{R_0}^{R_0+\Delta R} \frac{\mathrm{d}R}{u}$ for a radial expansion that occurs over a small distance ΔR of a few R_0. It yields $\tau_1 \sim \frac{\eta_0\ell^2}{k_BT}\left(\frac{R_0}{\ell}\right)^3$. This interpretation also clarifies the origin of the exponent $y_1 = -1$ for $\eta_{\mathrm{eff}} \sim \eta_0 N\left(\frac{R}{\ell}\right)^{y_1}$ during the globule expansion stage, as discussed in the theory and in section "Scaling form of free energy".

Moreover, the free energy $F \sim k_{\mathrm{B}}TN\left(\frac{\ell}{R}\right)^2$ is extensive; the estimated speed u is thus intensive (*i.e.* independent of N) and approximately $\frac{k_{\mathrm{B}}T}{\eta_0\ell}\left(\frac{\ell}{R}\right)^2$. This fact explains why the speed profile in the first stage depends on g_D but not on N, as shown in Fig. 11.

A closer examination of the simulations reveals that τ_1 and τ_2 in 2D space are approximately 1.5 times greater than those in 3D space, as illustrated in Fig. S8 of SI. This observation suggests a diffusive mechanism for the second stage of expansion. The expansion can be interpreted as a process that relaxes the chain from a non-equilibrium state. The relaxation is expected to complete within a time scale related to the chain diffusing over its size, expressed as $\tau_r \simeq \frac{R_f^2}{2d\mathcal{D}_{\mathrm{ch}}}$, where $\mathcal{D}_{\mathrm{ch}} \sim \frac{k_BT}{\eta_0 N}$ is the diffusion coefficient. Since the chain has the same equilibrium size R_f for both the 3D and 2D cases according to the FJC model (refer to Fig. 3), the factor of 1.5 can be derived between the two timescales, and the characteristic time exhibits an N^2 power-law dependence in both dimensions.

This work investigates a model system involving a chain expanding under theta conditions. It examines the Onsager's variational principle, verifies the free energy, and deepens our understanding of expansion kinetics. A robust theory has been developed that applies to both 3D and 2D spaces, providing profound insights into the behavior of polymers as they transition between confined and free states in a specific solvent environment.

The chain model studied in this work does not incorporate any bending rigidity. In reality, biological materials such as double-stranded DNA can exhibit significant persistence length ℓ_p, compared to flexible biopolymers like single-stranded DNA or single-stranded RNA. Therefore, it is crucial to further explore how the kinetics of expansion are influenced by ℓ_p, particularly when the size of a confining constraint becomes comparable to it. A practical approach for the investigation can be achieved by employing the Kratky–Porod model, which incorporates bending energy as $U_{\mathrm{bend}} = -k_BT\frac{\ell_p}{\ell}\sum_{i=1}^{N-1}\hat{\boldsymbol{b}}_{i+1}\cdot\hat{\boldsymbol{b}}_i$, where $\hat{\boldsymbol{b}}_i = \frac{\boldsymbol{r}_i - \boldsymbol{r}_{i-1}}{|\boldsymbol{r}_i - \boldsymbol{r}_{i-1}|}$ denotes the unit bond vector. The wormlike chain model is referred to as a continuous version of the Kratky–Porod model in the limit of $N \to \infty$ and $\ell \to 0$[43]. The investigation of chain rigidity and its impact on expansion kinetics will be a key focus of our future research.

Data availability

The datasets used or analyzed during the current study available from the corresponding author, P.-Y. H., on reasonable request.

Received: 24 November 2024; Accepted: 17 February 2025
Published online: 05 March 2025

References

1. Iwasa, J. & Marshall, W. *Karp's Cell and Molecular Biology* 8th edn. (Wiley, 2016).
2. Tortora, G. J., Funke, B. R. & Case, C. L. *Microbiology: An Introduction* 13th edn. (Pearson, 2018).
3. Greber, U. F. (ed.) *Physical Virology: Virus Structure and Mechanics* (Springer, 2019).
4. Taira, K. et al. (eds) *Non-viral Gene Therapy* (Springer, 2005).
5. Jayandharan, G. R. (ed.) *Gene and Cell Therapy: Biology and Applications* (Springer, 2018). https://doi.org/10.1007/978-981-13-0481-1.
6. Dunbar, C. E. et al. Gene therapy comes of age. *Science* **359**, 175. https://doi.org/10.1126/science.aan4672 (2018).
7. Nóbrega, C., Mendonça, L. & Matos, C. A. *A Handbook of Gene and Cell Therapy* (Springer International Publishing, 2020). https://doi.org/10.1007/978-3-030-41333-0.
8. Paunovska, K., Loughrey, D. & Dahlman, J. E. Drug delivery systems for RNA therapeutics. *Nat. Rev. Genet.* **23**, 265. https://doi.org/10.1038/s41576-021-00439-4 (2022).
9. Leandro, K. et al. Exploring the potential of cell-derived vesicles for transient delivery of gene editing payloads. *Adv. Drug Deliv. Rev.* **211**, 115346. https://doi.org/10.1016/j.addr.2024.115346 (2024).
10. Stockmayer, W. H. Problems of the statistical thermodynamics of dilute polymer solutions. *Makromol. Chem.* **35**, 54–74. https://doi.org/10.1002/macp.1960.020350103 (1960).
11. De Gennes, P. Collapse of a polymer chain in poor solvents. *J. Phys. Lett.* **36**, 55–57. https://doi.org/10.1051/jphyslet:0197500360305500 (1975).
12. Nishio, I., Sun, S.-T., Swislow, G. & Tanaka, T. First observation of the coil-globule transition in a single polymer chain. *Nature* **281**, 208–209. https://doi.org/10.1038/281208a0 (1979).
13. De Gennes, P. Kinetics of collapse for a flexible coil. *J. Phys. Lett.* **46**, 639 (1985).
14. Grosberg, A. Y., Nechaev, S. & Shakhnovich, E. The role of topological constraints in the kinetics of collapse of macromolecules. *J. Phys. Fr.* **49**, 2095. https://doi.org/10.1051/jphys:0198800490120209500 (1988).
15. Birshtein, T. M. & Pryamitsyn, V. A. Coil-globule type transitions in polymers. 2. Theory of coil-globule transition in linear macromolecules. *Macromolecules* **24**, 1554–1560. https://doi.org/10.1021/ma00007a017 (1991).
16. Klushin, L. I. Kinetics of a homopolymer collapse: Beyond the Rouse-Zimm scaling. *J. Chem. Phys.* **108**, 7917. https://doi.org/10.1063/1.476229 (1998).
17. Abrams, C. F., Lee, N.-K. & Obukhov, S. P. Collapse dynamics of a polymer chain: Theory and simulation. *Europhys. Lett.* **59**, 391–397. https://doi.org/10.1209/epl/i2002-00207-5 (2002).
18. Sherman, E. & Haran, G. Coil-globule transition in the denatured state of a small protein. *Proc. Natl. Acad. Sci. USA* **103**, 11539–11543. https://doi.org/10.1073/pnas.0601395103 (2006).
19. Maffi, C., Baiesi, M., Casetti, L. & Piazza, F. First-order coil-globule transition driven by vibrational entropy. *Nat. Commun.* **3**, 1065. https://doi.org/10.1038/ncomms2055 (2012).
20. Majumder, S., Zierenberg, J. & Janke, W. Kinetics of polymer collapse: effect of temperature on cluster growth and aging. *Soft Matter* **13**, 1276–1290. https://doi.org/10.1039/c6sm02197b (2017).
21. Xu, Y. & Wang, Z.-G. Coil-to-globule transition in polymeric solvents. *Macromolecules* **54**, 10984–10993. https://doi.org/10.1021/acs.macromol.1c01748 (2021).
22. Singh, T. V. & Shagolsem, L. S. Universality and identity ordering in heteropolymer coil-globule transition. *Macromolecules* **55**, 10457–10467. https://doi.org/10.1021/acs.macromol.2c01559 (2022).
23. Polanowski, P. & Sikorski, A. Coil-globule transition in two-dimensional polymer chains in an explicit solvent. *Soft Matter* **19**, 7979–7987. https://doi.org/10.1039/d3sm00975k (2023).
24. Grosberg, A. R. & Khokhlov, A. Y. *Statistical Physics of Macromolecules* (AIP Press, 1994).
25. Zhang, G. & Wu, C. Reentrant coil-to-globule-to-coil transition of a single linear homopolymer chain in a water/methanol mixture. *Phys. Rev. Lett.* **86**, 822–825. https://doi.org/10.1103/physrevlett.86.822 (2001).
26. Budkov, Y. A., Kolesnikov, A. L., Kalikin, N. N. & Kiselev, M. G. A statistical theory of coil-to-globule-to-coil transition of a polymer chain in a mixture of good solvents. *Europhys. Lett.* **114**, 46004. https://doi.org/10.1209/0295-5075/114/46004 (2016).
27. Inoue, M., Hayashi, T., Hikiri, S., Ikeguchi, M. & Kinoshita, M. Mechanism of globule-to-coil transition of poly(n-isopropylacrylamide) in water: Relevance to cold denaturation of a protein. *J. Mol. Liq.* **292**, 111374. https://doi.org/10.1016/j.molliq.2019.111374 (2019).
28. Lu, H., Xing, Z., Hossain, M. & Leng, J. Scaling dynamics of globule-to-coil phase transition in double-network hydrogel with ultra-high stretchable strength. *Smart Mater. Struct.* **29**, 085050. https://doi.org/10.1088/1361-665x/ab9e0c (2020).
29. Paul, S., Majumder, S. & Janke, W. Activity mediated globule to coil transition of a flexible polymer in a poor solvent. *Soft Matter* **18**, 6392–6403. https://doi.org/10.1039/d2sm00354f (2022).
30. Wu, C. & Wang, X. Globule-to-coil transition of a single homopolymer chain in solution. *Phys. Rev. Lett.* **80**, 4092. https://doi.org/10.1103/physrevlett.80.4092 (1998).
31. Wang, X., Qiu, X. & Wu, C. title Comparison of the coil-to-globule and the globule-to-coil transitions of a single poly(N-isopropylacrylamide) homopolymer chain in water. *Macromolecules* **31**, 2972. https://doi.org/10.1021/ma971873p (1998).
32. Pitard, E. & Orland, H. Dynamics of the swelling or collapse of a homopolymer. *Europhys. Lett.* **41**, 467. https://doi.org/10.1209/epl/i1998-00175-8 (1998).
33. Lee, N.-K., Abrams, C. F., Johner, A. & Obukhov, S. Arrested swelling of highly entangled polymer globules. *Phys. Rev. Lett.* **90**, 225504. https://doi.org/10.1103/physrevlett.90.225504 (2003).
34. Lee, N.-K., Abrams, C. F., Johner, A. & Obukhov, S. Swelling dynamics of collapsed polymers. *Macromolecules* **37**, 651. https://doi.org/10.1021/ma034808q (2004).
35. Sakaue, T. & Yoshinaga, N. Dynamics of polymer decompression: Expansion, unfolding, and ejection. *Phys. Rev. Lett.* **102**, 148302. https://doi.org/10.1103/physrevlett.102.148302 (2009).
36. Nakata, M., Nakamura, Y., Sasaki, N. & Maki, Y. Slow knot formation by suppressed self-reptation in a collapsed polymer chain. *Phys. Rev. E* **85**, 021802. https://doi.org/10.1103/physreve.85.021802 (2012).
37. Nakata, M., Nakamura, Y., Maki, Y. & Dobashi, T. Chain expansion process from knotted globule. *Polymer* **178**, 121541. https://doi.org/10.1016/j.polymer.2019.06.007 (2019).
38. Chu, C.-C. & Hsiao, P.-Y. Expansion of single chains released from a spherical cavity. *Polymers* **15**, 198. https://doi.org/10.3390/polym15010198 (2023).
39. Hsiao, P.-Y. Expansion kinetics of flexible polymers upon release from a disk-shaped confinement. *ACS Omega* **9**, 13797–13802. https://doi.org/10.1021/acsomega.3c08378 (2024).
40. Buchta, D. et al. Enterovirus particles expel capsid pentamers to enable genome release. *Nat. Commun.* **10**, 1138. https://doi.org/10.1038/s41467-019-09132-x (2019).
41. Škubník, K. et al. Capsid opening enables genome release of iflaviruses. *Sci. Adv.* **7**, eabd7130. https://doi.org/10.1126/sciadv.abd7130 (2021).
42. Sukeník, L. et al. Cargo release from nonenveloped viruses and virus-like nanoparticles: Capsid rupture or pore formation. *ACS Nano* **15**, 19233. https://doi.org/10.1021/acsnano.1c04814 (2021).
43. Rubinstein, M. & Colby, R. H. *Polymer Physics* (Oxford University Press, 2003).
44. Teraoka, I. *Polymer Solutions: An Introduction to Physical Properties* (Wiley, 2002).
45. Marko, J. F. & Siggia, E. D. Stretching DNA. *Macromolecules* **28**, 8759–8770. https://doi.org/10.1021/ma00130a008 (1995).

46. Doi, M. & Edwards, S. *The Theory of Polymer Dynamics* (Clarendon Press, 1986).
47. Doi, M. Onsager's variational principle in soft matter. *J. Phys. Condens. Matter* **23**, 284118. https://doi.org/10.1088/0953-8984/23/28/284118 (2011).
48. Doi, M. *Soft Matter Physics* (Oxford University Press, 2013). https://doi.org/10.1093/acprof:oso/9780199652952.001.0001.
49. Grosberg, A. Y. & Kuznetsov, D. V. Quantitative theory of the globule-to-coil transition. 1. Link density distribution in a globule and its radius of gyration. *Macromolecules* **25**, 1970–1979. https://doi.org/10.1021/ma00033a022 (1992).
50. Thompson, A. P., Aktulga, H. M., Berger, R., Bolintineanu, D. S., Brown, W. M., Crozier, P. S., in't Veld, P. J., Kohlmeyer, A., Moore, S. G., Nguyen, T. D., Shan, R., Stevens, M. J. Tranchida, J., Trott, C., & Plimpton, S. J. Lammps - a flexible simulation tool for particle-based materials modeling at the atomic, meso, and continuum scales. Comput. Phys. Commun. **271**, 108171 (2022). https://doi.org/10.1016/j.cpc.2021.108171. Refer also to LAMMPS website at http://lammps.sandia.gov/
51. Bishop, M. & Saltiel, C. J. Application of the pivot algorithm for investigating the shapes of two- and three-dimensional lattice polymers. *J. Chem. Phys.* **88**, 6594–6596. https://doi.org/10.1063/1.454446 (1988).
52. Jagodzinski, O., Eisenriegler, E. & Kremer, K. Universal shape properties of open and closed polymer chains: renormalization group analysis and Monte Carlo experiments. *J. Phys. I* **2**, 2243. https://doi.org/10.1051/jp1:1992279 (1992).
53. Steinhauser, M. O. A molecular dynamics study on universal properties of polymer chains in different solvent qualities. Part I. A review of linear chain properties. *J. Chem. Phys.* **122**, 094907. https://doi.org/10.1063/1.1846651 (2005).

Acknowledgements

This material is based upon work supported by National Science and Technology Council, Taiwan under the contract No. NSTC 112-2112-M-007-019 and NSTC 113-2112-M-007-010.

Author contributions

P.-Y. H. is the only author who contributes to the entire work.

Declarations

Competing interests

The author declares no competing interests.

Additional information

Supplementary Information The online version contains supplementary material available at https://doi.org/10.1038/s41598-025-90891-7.

Correspondence and requests for materials should be addressed to P.-Y.H.

Reprints and permissions information is available at www.nature.com/reprints.

Publisher's note Springer Nature remains neutral with regard to jurisdictional claims in published maps and institutional affiliations.